Indian Journal of Chemistry
Vol. 57A, June 2018, pp. 784-790

Effect of γ-radiation on structure, photoluminescence properties and *in vitro* cytotoxicity of $LaPO_4:Tb^{3+},Ce^{3+}$ phosphor

Vema Reddy Bheeram[a], Sudheer Gurugubelli[a], Anima S Dadhich[a], Anil Kumar Badana[b], Rama Rao Malla[b], Abhijit Saha[c] & Saratchandra Babu Mukkamala[a,*]

[a]Department of Chemistry, GIS, GITAM (Deemed University), Visakhapatnam 530 045, AP, India

Email: mscbabu@yahoo.com

[b]Department of Biochemistry and Bioinformatics, GITAM (Deemed University), Visakhapatnam 530 045, AP, India

[c]UGC-DAE consortium for Scientific Research, Kolkata 700 098, WB, India

Received 9 June 2017; re-revised and accepted 22 May 2018

Lauric acid capped Ce^{3+} sensitized $LaPO_4:Tb^{3+}$ nanorods have been synthesized by hydrothermal route at 150 °C. The structure, stability and luminescent properties have been examined by TEM, TG/DTA, FT-IR, powder X-ray diffraction and PL spectral data. Cytotoxic activity has been examined by MTT assay. The $LaPO_4:Tb^{3+},Ce^{3+}$ phosphor exhibits four emission peaks at 485, 551, 583 and 619 nm corresponding to $^5D_4 \rightarrow {}^7F_6$, $^5D_4 \rightarrow {}^7F_5$, $^5D_4 \rightarrow {}^7F_4$ and $^5D_4 \rightarrow {}^7F_3$ transitions, respectively. The influence of γ-radiation on photoluminescence properties of $LaPO_4:Tb^{3+},Ce^{3+}$ phosphor has also been examined at 5 and 300 kGy. Furthermore, $LaPO_4$ and $LaPO_4:Tb^{3+},Ce^{3+}$ phosphors exhibit 80–82% cytotoxic effect against breast cancer cell lines, MDA-MB 231 and MCF-7. The IC_{50} values for $LaPO_4$ and $LaPO_4:Tb^{3+},Ce^{3+}$ phosphors are 17.2 and 13.5 µg/mL against MCF-7 and 21.5 and 15.0 µg/mL against MDA-MB 231 cell line, respectively.

Keywords: Phosphors, Hydrothermal synthesis, Luminescence, Gamma radiations, Cytotoxicity, Lanthanum phosphates, Rare earths, Cerium, Terbium

Rare-earth (RE^{3+}) doped lanthanum phosphates ($LaPO_4:RE^{3+}$) have received significant attention due to their unique properties and are used in plasma display panels (PDPs)[1,2], fluorescent lamps[3], microelectronic devices[4] and biomedical applications[5,6]. Lanthanum phosphate ($LaPO_4$) has high specific melting point and surface area as compared to other conventional phosphate based materials[7]. Furthermore, in general RE^{3+} doped orthophosphates normally exhibit high stability under both acidic and basic conditions[8,9]. The embedded RE^{3+} element in phosphate material is known to influence the optical properties of the host material[10]. In particular, the addition of green light emitting trivalent terbium (Tb^{3+}) with an electron configuration $4f^8$ is well known to upgrade the fluorescence properties of doped phosphates[11,12]. Co-activation of several lanthanide cations like Ce^{3+} (as a sensitizer), is known to increase the luminescence intensities of various nanophosphors[13] like Ce^{3+} and Sm^{3+} co-doped YAG phosphors, Ce^{3+} co-activated $LaPO_4:Dy^{3+},Ce^{3+}$ sensitized $YPO_4:Eu^{3+}$ and $YPO_4:Dy^{3+}$. However, crystalline materials of rare earth ions exhibit more fluorescence as compared to the amorphous materials. Various synthetic processes including co-precipitation, combustion, sol-gel, high temperature solid state reactions and hydro/solvo-thermal techniques are reported in the literature for the synthesis of phosphors. Among these methods, hydro/solvo-thermal method is known to give pure nanocrystals of uniform size and shape, with high degree of crystallinity[14-16].

Further, exposure of surface of nanocrystals to high energy ionization radiation (X-rays, γ-rays) may result in displacement of atoms from their own positions, depending on the energy of ionization radiation[17]. Also, non-linear interaction of electronic excitations by ionization radiation can play an important role in luminescence performance of materials[18].

Rare-earth based nanoparticles are of increasing importance in cancer diagnosis and therapy due to the versatile chemical, optical and biocompatible features such as tunable emission colours, high photochemical stability, long luminescent lifetime and ET processes between dopants[19-22]. Breast cancer is the most frequently diagnosed cancer in women and one of the leading causes of cancer death for women. About 1.3 million cases of breast cancer are diagnosed and 4,50,000 women die annually throughout the world[23]. Rare-earth doped nanoparticles show almost no toxicity upon incubation with human cell line, i.e., HeLa cells[22], but exhibit toxicity against human skin cell[24].

This study reports the effect of γ-radiation on structural and optical properties of $LaPO_4:Tb^{3+},Ce^{3+}$ phosphor at doses of 5 and 300 kGy. In addition, the cytotoxic effect on breast cancer cell lines is also evaluated.

Experimental

All chemicals were of analytical grade and used without any further purification. $Tb(NO_3)_3.6H_2O$ was purchased from Sigma-Aldrich, USA, $La(NO_3)_3.6H_2O$ and $Ce(NO_3)_3.6H_2O$ from Acros Organics, Belgium, Disodium hydrogen phosphate, Lauric acid and DMSO (Dimethyl sulfoxide) from Merck, India. DMEM, FBS, Penicillin and streptomycin, 0.05% Trypsin-EDTA were procured from Invitrogen, USA. The human breast epithelial adenocarcinoma cell lines, MDA-MB-231 and MCF-7, were obtained from the National Center for Cell Science, Pune, India. The cells were grown up to 70% confluence in DMEM supplemented with 10% FBS, penicillin–streptomycin (100 µg/mL) in a humid atmosphere of 5% CO_2 at 37 °C.

The TG measurements were carried out on a Melter Toledo TGA/DSC-1 apparatus. The sample (50 mg) was heated in the temperature ranging from 30–1000 °C at a heating rate of 10 °C/min in a pan under nitrogen atmosphere. FT-IR spectrum was recorded at room temperature using KBR pellet method on a Perkin Elmer "Spectrum Two" FT-IR spectrophotometer. Raman spectrum was recorded using Lab Ram HR 800 full automatic confocal Raman microscope (Horiba Jobin Yvon). The Raman signal was investigated within the range 1000–3000 cm^{-1}. Luminescence spectrum of the solid sample was recorded using a Perkin Elmer LS-55 luminescence spectrometer at room temperature. Powder X-ray diffraction (PXRD) pattern was recorded on Panalytical X'Pert pro powder X-ray diffractometer, with graphite monochromatic Cu-K_α (λ = 1.5406 Å) radiation and generator settings at 40 kV and 30 mA at room temperature. Transmission electron microscopy (TEM) images were recorded on a Philips CM-200 instrument. EDX analysis was carried out by field emission scanning electron microscopy (Hitachi S-4800 SEM). The cell images were captured with an Olympus IX53 inverted microscope. For γ-radiation measurements, all the obtained samples were divided into small portions and packed in plastic vials with para film. These samples were exposed to gamma radiation using a ^{60}Co gamma cell (^{60}Co-source capacity 3700 Ci) at a dose rate 2.95 kGy/h at room temperature. All the samples were irradiated by γ-radiation at doses of 5 and 300 kGy.

Millipore-Q purified water was used throughout the synthesis. Standard stock solutions (0.2 M) of $La(NO_3)_3.6H_2O$, $Tb(NO_3)_3.6H_2O$ and $Ce(NO_3)_3.6H_2O$ were prepared. Then, 2.0 mmol lauric acid (10 mL, 0.2 M), 5.0 mL ethanol and 0.6 g sodium hydroxide were taken in a 50 mL beaker and stirred continuously for 15 min to prepare the capping agent, i. e., sodium laurate. To this capping agent, 1.0 mmol of disodium hydrogen orthophosphate solution (5.0 mL, 0.2 M) and 1.0 mmol of $La(NO_3)_3.6H_2O$ (5.0 mL, 0.2 M) were added and stirred for 30 min until a transparent solution was obtained. Then, the resulting solution was transferred into a 23.0 mL Teflon lined stainless steel autoclave and heated solvothermally at 150 °C for 12 h. After cooling down to room temperature, the gelatinous product was separated by centrifugation, washed with ethanol and deionized water several times and dried in oven under air at 60 °C. For synthesis of RE^{3+} doped $LaPO_4$, $La(NO_3)_3.6H_2O$ (1, 5 or 10%) was replaced with $Tb(NO_3)_3.6H_2O$ (10%) and $Ce(NO_3)_3.6H_2O$ (1 or 5%).

The cytotoxicity of the nanomaterials against MDA-MB 231 and MCF-7 cells[25] was evaluated by MTT assay. The synthesized phosphors were suspended in complete DMEM media at 5, 10, 15, 20 and 25 µg/mL (*w/v*) and was used to treat overnight grown cells (1×10^4/well) for 24 and 48 h. After treatment, 20 µL of MTT solution (5 mg/mL) was added and incubated for 3 h followed by 100 µL of DMSO. Untreated wells served as control. The absorbance was measured at 570 nm using ELISA reader. The cytotoxicity (%) was calculated as follows: [(O.D. of treated wells – O.D. of blank wells)/(O.D. of control wells – O.D. of blank wells)]×100.

Cell morphology was examined by phase contrast microscopy. The cells were left untreated or treated with nanomaterials at 15 and 25 µg/mL for 48 h. The medium was removed and the cells were washed three times with PBS. The cell images were captured under the phase contrast inverted microscope.

Results and discussion

The size and morphology of the synthesized $LaPO_4:Tb^{3+},Ce^{3+}$ phosphor was examined by transmission electron microscopy (TEM) as shown in Fig. 1(a, b). After doping the RE^{3+} (Tb^{3+} or Ce^{3+}) into phosphate host, no prominent morphological changes were observed in $LaPO_4$. The $LaPO_4:Tb^{3+},Ce^{3+}$ exhibited uniform hexagonal rod shaped morphology of width and length ~40 and ~300 nm, respectively. In addition, a comprehensive view of the phase pattern of the sample was obtained

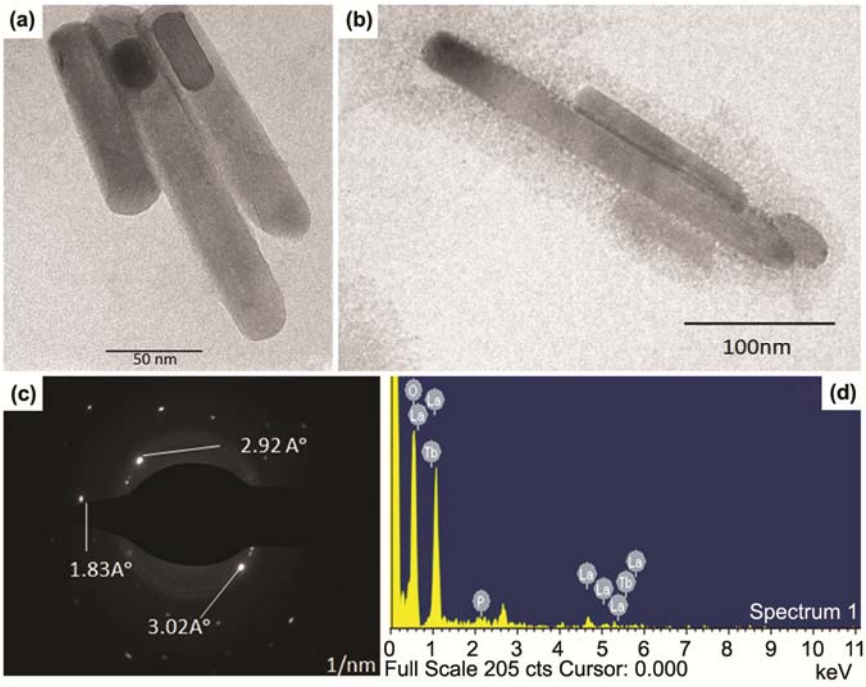

Fig. 1 – (a & b) TEM images of $LaPO_4:Tb^{3+}$, Ce^{3+}, (c) SAED pattern of $LaPO_4:Tb^{3+},Ce^{3+}$, and, (d) EDX analysis of $LaPO_4:Tb^{3+},Ce^{3+}$ phosphor.

by SAED. The SAED patterns of $LaPO_4:Tb^{3+},Ce^{3+}$ phosphor demonstrated almost clear reflections, suggesting high-quality crystalline nature of the $LaPO_4$. As shown in Fig. 1c, the interplanar spacing (*d*-spacing/ *hkl* values) of $LaPO_4:Tb^{3+},Ce^{3+}$ phosphor matched with powder XRD patterns of $LaPO_4$ (ICDD-PDF 46-1439). The EDX spectrum of $LaPO_4:Tb^{3+},Ce^{3+}$ phosphor confirmed the presence of La, P, Tb and O (Fig. 1d). The percentage of elements ratio (M/P/O) obtained from the EDX spectrum is almost similar to the standard La/P/O atom ratio (1:1:4) of pure $LaPO_4$ phase.

The crystallinity, phase purity and influence of dopant on the product was examined by powder X-ray diffraction analysis (PXRD). Figure 2 shows the PXRD patterns of $LaPO_4$ and $LaPO_4$: Tb^{3+},Ce^{3+} phosphors. The PXRD pattern of the $LaPO_4$: Tb^{3+},Ce^{3+} phosphor was in good agreement with the values of $LaPO_4.0.5H_2O$ (ICDD-PDF 46-1439), which exhibited hexagonal phase of $LaPO_4$. Furthermore, no additional peaks for other phases associated with the doped component were observed, indicating that some of the Ln^{3+} ions were replaced with Tb^{3+} and Ce^{3+} ions (radius: La^{3+} = 1.16 Å, Tb^{3+} = 1.04 Å, Ce^{3+} = 1.14 Å). In addition, it should be noted that the synthesized rare earth doped $LaPO_4$ samples showed very minor changes in the diffraction peaks as compared to the standard data (this may be due to the small differences

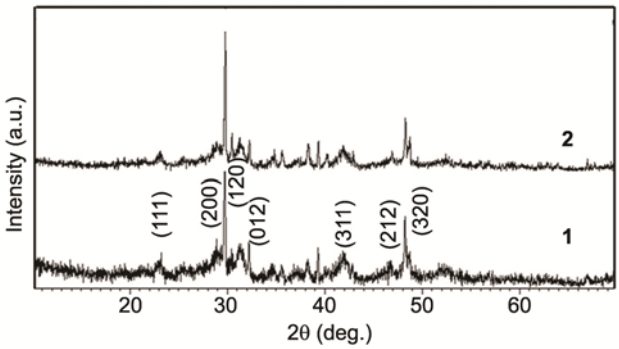

Fig. 2 – Powder XRD patterns of (1) $LaPO_4$, and, (2) $LaPO_4:Tb^{3+},Ce^{3+}$ phosphors.

in their ionic radii). Due to similar ionic radius and valence of the rare earth cations, it is, therefore, suggested that Tb^{3+} and Ce^{3+} ions preferably occupy the La^{3+} sites. Influence of γ-radiation on $LaPO_4:Tb^{3+},Ce^{3+}$ phosphors was examined at 5 and 300 kGy doses to identify the structural stability of the phosphors. The powder XRD patterns of $LaPO_4:Tb^{3+},Ce^{3+}$ phosphor were recorded before and after γ-irradiation (and normalized w.r.t. the highest intensity in each pattern). After γ-irradiation at 5 kGy and 300 kGy, no change in the peak position was observed except for a little change in the peak intensity. This indicates that γ-radiation had no effect on the crystal structure of $LaPO_4:Tb^{3+},Ce^{3+}$ phosphor (Supplementary data, Fig. S1).

The FT-IR spectra of $LaPO_4$ and $LaPO_4:Tb^{3+},Ce^{3+}$ phosphors shows the O-H stretching vibration at 3459 cm^{-1} assigned to water molecules (Supplementary data, Fig. S2). The peaks at 2926 and 2850 cm^{-1} are assigned to the symmetric and asymmetric methylene stretches of alkyl groups. The peak at 1076 cm^{-1} is a characteristic asymmetric stretching of P–O band (commonly known as υ_3 region), while the two peaks located at 615 and 540 cm^{-1} may be assigned to the υ_4 region of the vibrations of phosphate groups. The shoulder at 952 cm^{-1} may be assigned to the υ_4 vibration of phosphate groups. Furthermore, a broad peak centered at 1385 cm^{-1} may be assigned to C-H stretching vibrations, indicating the presence of lauric acid on the surface of the synthesized materials.

The FT-IR absorption spectra of $LaPO_4:Tb^{3+},Ce^{3+}$ phosphor was recorded before and after γ-irradiation at a dose of 5 kGy and 300 kGy. After γ-irradiation, increase in the intensity of the absorption curves was initially observed at the first dose of 5 kGy, which further increased progressively on increasing the dose to 300 kGy. The obtained infrared results indicated that, after irradiation, the elementary structure remained unchanged (Supplementary data, Fig. S3).

The Raman band at 1085 cm^{-1} corresponding to ν(C-C) stretching vibrations and peaks centered at 1440 and 1658 cm^{-1} are attributed to ν(CH_2) wagging vibrations and typical carbonyl stretching frequencies of ν(C=O) in $LaPO_4$ (Supplementary data, Fig. S4).

TG-DTA measurements were carried out to investigate the thermal stability of hexagonal $LaPO_4$ (Fig. 3). Three main distinguished weight losses were observed in TGA analysis of $LaPO_4$ sample. The first stage of weight loss (12.6%) can be assigned to the loss of absorbed water molecules between 25–100 °C. The second stage of widespread weight loss of about 10.2% at temperature 380–410 °C can be attributed to the crystallization as well as removal of organic moiety. A strong exothermic peak at about 370 °C indicates the crystallization of $LaPO_4$. Thereafter, the mass loss decreased progressively and ended at 900 °C, which appears to be the decomposition of residual nitrates in the precursor.

The emission spectra of the RE doped $LaPO_4$ phosphor, after photoexcitation at 231 nm, are shown in Fig. 4. $LaPO_4$ serves as host lattice, while Tb^{3+} ions act as activator and Ce^{3+} ion as co-activator. Four strong emission bands were observed for terbium doped $LaPO_4$ system in the range 450–700 nm. Four characteristic peaks at 485, 551, 583 and 619 nm

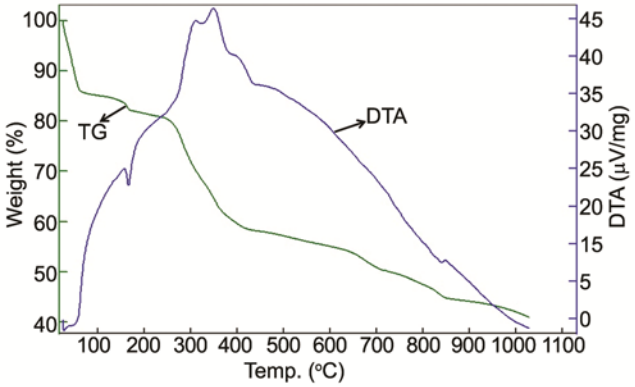

Fig. 3 – TG-DTA profile of $LaPO_4$.

corresponding to $^5D_4 \rightarrow {}^7F_6$, $^5D_4 \rightarrow {}^7F_5$, $^5D_4 \rightarrow {}^7F_4$ and $^5D_4 \rightarrow {}^7F_3$ transitions, respectively.

The luminescence emissions from Tb^{3+} ions generally originate within the 4*f* shell. $LaPO_4$ was a desirable host matrix for Tb^{3+} ions, and while incorporating the Tb^{3+} ions into $LaPO_4$ nanoparticles, they simply acted as activators and produced corresponding characteristic emissions through efficient energy transfer from the $LaPO_4$ host to the dopants. As shown in the Fig. 4a, addition of Ce^{3+} ions (1–5%) to $LaPO_4:Tb^{3+}$ phosphor did not affect its peak positions in PL spectra; however, luminescence intensity increased progressively[26].

The influence of γ-radiation on photoluminescent behavior of $LaPO_4:Tb^{3+}$, $LaPO_4:Tb^{3+},Ce^{3+}$(1%) and $LaPO_4:Tb^{3+},Ce^{3+}$(5%) phosphors was examined and results are shown in Fig. 4(b-d). After γ-irradiation, no shift in the emission wavelength was observed. However, progressive decrease in the emission intensity was observed on increasing the radiation dose from 5 kGy to 300 kGy. The decrease in photoluminescence intensity may be due to loss of heat energy through non-radiative processes[27].

Cytotoxicity is typically used to evaluate the effect of nanomaterials on cell proliferation. As a preliminary study, the cytotoxic effect of nanomaterials was evaluated in the concentration range from 5-25 μg/mL. The results suggest that $LaPO_4$ caused 10, 19, 30, 37 and 54% cytotoxicity in MDA-MB-231 cells after 24 h treatment and 13, 24, 38, 49 and 70% cytotoxicity after 48 h of treatment at 5, 10, 15, 20 and 25 μg/mL concentration, respectively (Supplementary data, Fig. S5(a)). As shown in Fig. S5(b), $LaPO_4$ caused 13, 28, 34, 44 and 58% and 18, 30, 44, 64 and 80% cytotoxicity after 24 h and 48 h in MCF-7 cells, respectively. On the other hand, the $LaPO_4:Tb^{3+}$, Ce^{3+} phosphor

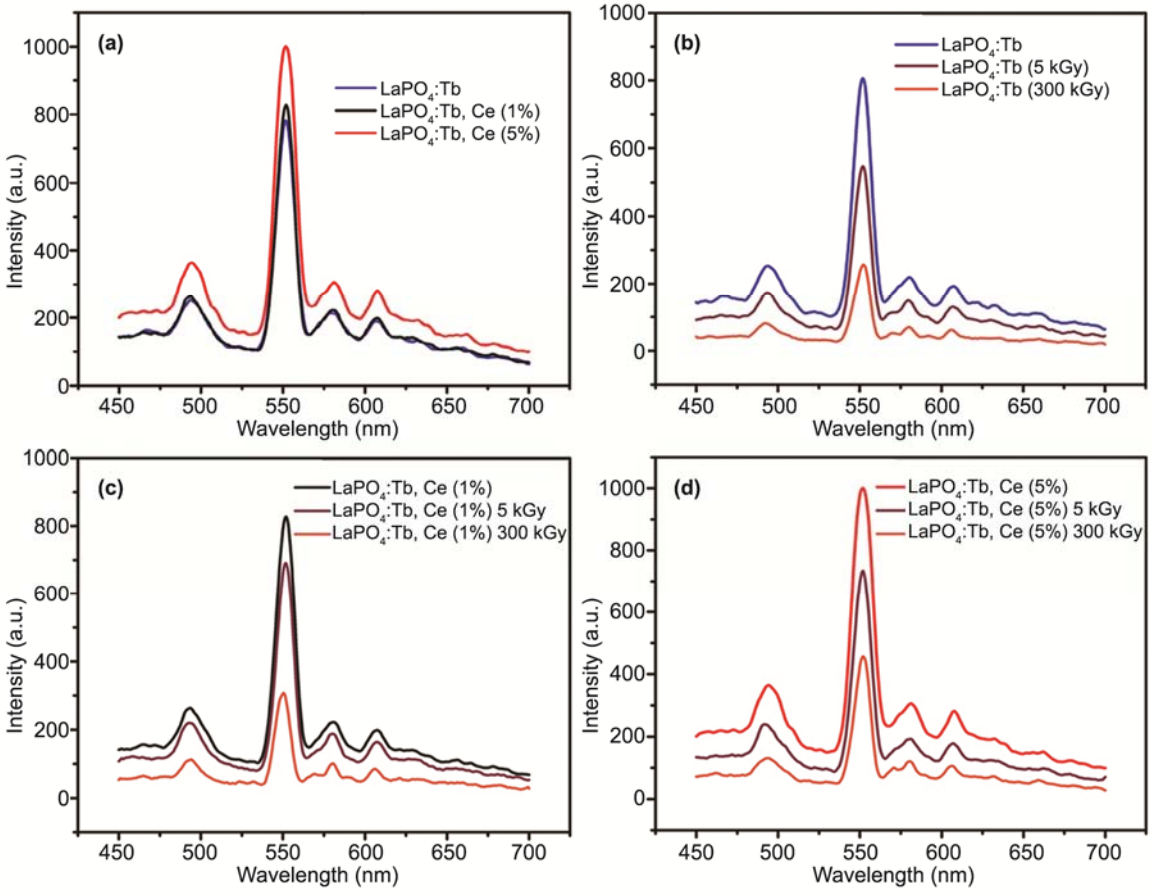

Fig. 4 – Photoluminescence spectra of RE-doped phosphors. [(a) Pre-irradiated RE-doped phosphors; (b) γ-irradiated $LaPO_4:Tb^{3+}$; (c) γ-irradiated $LaPO_4:Tb^{3+},Ce^{3+}$(1%); (d) γ-irradiated $LaPO_4:Tb^{3+},Ce^{3+}$(5%)].

(Fig. S5(c)) caused 5, 9, 15, 26 and 37% and 15, 25, 38, 51 and 72% cytotoxicity after 24 and 48 h treatment of MDA-MB-231 cells, respectively, at the same concentrations. As shown in Figure S5(d), the Tb^{3+}, Ce^{3+} doped lanthanum phosphate ($LaPO_4:Tb^{3+},Ce^{3+}$) caused 12, 23, 30, 44 and 62% and 16, 34, 57, 65 and 80% cytotoxicity after 24 and 48 h treatment of MCF-7 cells, respectively, at the same concentration.

The IC_{50} values of $LaPO_4$ against MCF-7 and MDA-MB 231 cell lines were found to be 17.2 and 21.5 µg/mL, respectively, while, IC_{50} values of $LaPO_4:Tb^{3+}$, Ce^{3+} phosphor against MCF-7 and MDA-MB 231 cell lines were found to be 13.5 and 15.0 µg/mL at 48 h treatment. These results indicate that the concentration of nanomaterials required for inhibition of 50% growth of both MCF-7 and MDA-MB 231 cell lines decreased due to doping of $LaPO_4$ with Tb^{3+}, Ce^{3+}. The viability of normal breast epithelial cell line, MCF-12A treated with both $LaPO_4$ and $LaPO_4:Tb^{3+}$, Ce^{3+} phosphor was > 97% suggesting that these nanomaterials are not toxic at 15 µg/mL. However, mild reduction of cell viability (~92.5%) occurred at 25 µg/mL (data not shown). These results indicate that both $LaPO_4$ and $LaPO_4:Tb^{3+},Ce^{3+}$ phosphor are specific to cancer cells.

Further, to evaluate the effect of nanomaterials on the growth of breast cancer cell lines, morphology of cells was observed under a phase contrast microscope. The result showed that $LaPO_4$ altered the morphology of MDA-MB-231 and MCF-7 in a concentration dependent manner (Fig. 5). $LaPO_4:Tb^{3+},Ce^{3+}$ phosphor also changed the morphology of MDA-MB-231 and MCF-7 (Fig. 6).

These results indicate that both compounds enhanced the cytotoxicity against both breast cancer cell lines, MDA-MB-231 and MCF-7, in a dose and time dependent manner. $LaPO_4:Tb^{3+},Ce^{3+}$ phosphor shows marginal increase or same toxicity (72% and 80%) compared to the host material $LaPO_4$ (70% and 80%) on MDA-MB-231 and MCF-7 cells. In addition, size of nanoparticles also played an important role in

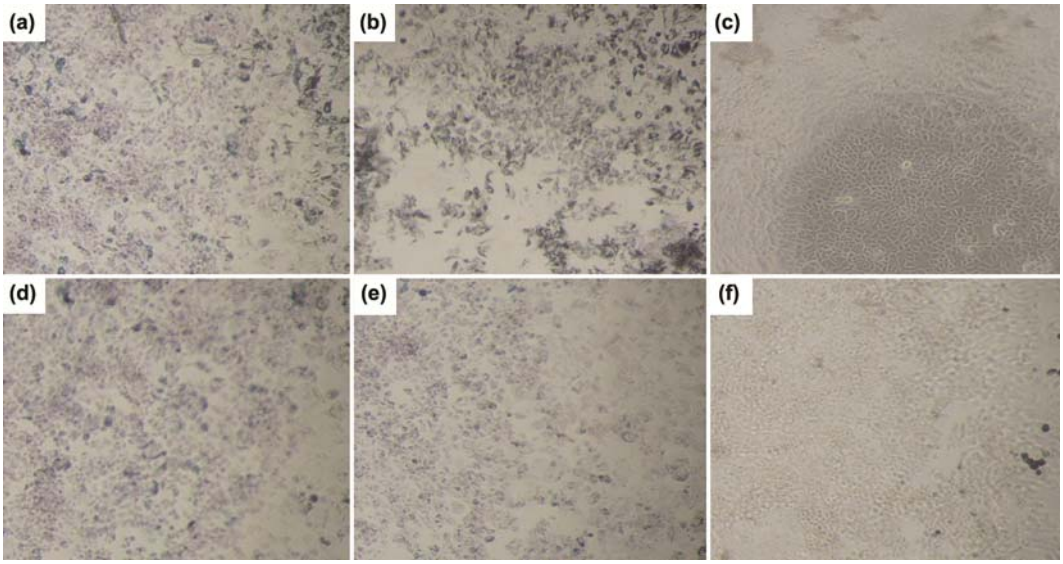

Fig. 5 – Effect of $LaPO_4$ on growth of MDA-MB-231 (a, b, c) and MCF-7 cells (d, e, f) at 48 h treatment. [a & d = Controls; b & e = 15 µg/mL; c & f = 25 µg/mL].

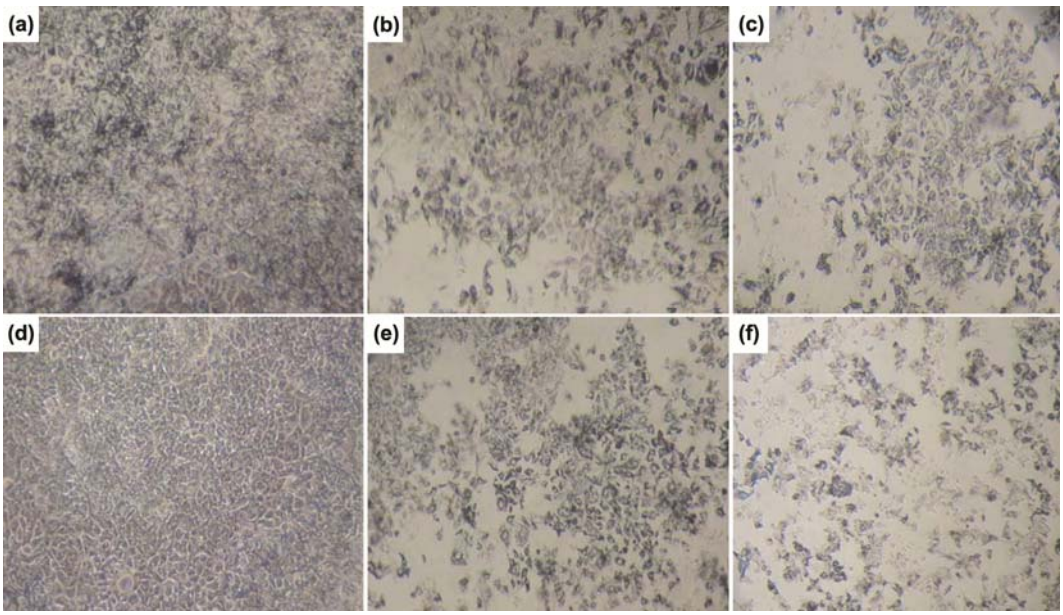

Fig. 6 – Effect of $LaPO_4:Tb^{3+},Ce^{3+}$ phosphor on growth of MDA-MB-231 (a, b, c) and MCF-7 cells (d, e, f) at 48 h treatment. [a & d = Controls; b & e = 15 µg/mL; c & f = 25 µg/mL].

treatment of cancer cells[28]. Nanoparticles with about 50–100 nm size is optimal for accumulation on tumor tissue and release of the reactive oxygen species (ROS) to destroy the cancer cells. From these studies, it appears that the $LaPO_4:Tb^{3+},Ce^{3+}$ phosphor is also a suitable candidate for treatment of cancer.

In summary, Ce^{+3} co-doped $LaPO_4:Tb^{3+}$ phosphor was synthesized through hydrothermal route in mixed solvents of ethanol and water at relatively low temperature. The $LaPO_4:Tb^{3+},Ce^{3+}$ phosphor exhibits uniform hexagonal rods with length and width around 300 nm and 40 nm, respectively. All materials exhibit high thermal stability after γ-irradiation at 5 and 300 kGy. Quenching of PL intensity was observed after γ-ray exposure. $LaPO_4$ and $LaPO_4:Tb^{3+},Ce^{3+}$ phosphors caused significant cytotoxicity and affected the morphology of human breast epithelial adenocarcinoma cell lines.

Supplementary data

Supplementary data associated with this article are available in the electronic form at http://www.niscair.res.in/jinfo/ijca/IJCA_57A(06)784-790_SupplData.pdf.

Acknowledgement

The authors are thankful to UGC-DAE consortium for Scientific Research, Kolkata Centre, India, for financial support (Project no. UGC-DAE-CSR-KC/ CRS/13/RC08/ 0891).

References

1 Pimpalshende D M, Dhoble S, *J Lumin*, 30 (2015) 144.
2 Wang D, Shun Q, Wang Y & Zhang Z, *Mater Chem Phys*, 147 (2014) 831.
3 Guo D, Hu C & Xi Y, *Appl Sur Sci*, 268 (2013) 458.
4 Ghosh P, Patra A, *J Nanosci Nanotechnol,* 8 (2008) 3458.
5 Ghosh R, Sarkar R & Paul S, *Mater Design*, 106 (2016) 161.
6 Tehrani S M, Lin W, Rosenfeldt S, Guerin G, Lu Y, Liang Y, Drechsler M, Forster S & Winnik A M, *Chem Mater*, 28 (2016) 501.
7 Onoda H & Funamoto T, *J Mater Res Technol*, 3 (2014) 122.
8 Rajesh K, Shajesh P, Seidei O, Mukundan P & Warrier K G K, *Adv Funct Mater*, 17 **(**2007) 1682.
9 Onoda H, Taniguchi K & Tanaka I, *Microporous Mesoporous Mater,* 109 (2008) 193.
10 Li Y, Ma H, Hua Y, Yand Q, Li C, Deng D & Xu S, *J Rare Earths*, 34 (2016) 7.
11 Houa D, Guo X, Liu C, Sham T, Liang H, Gao J, Sun X, Zhang B, Zhan F, Huan Y & Tao Y*, J Lumin*, 165 (2015) 23.
12 Liu Y, Yang C, Xiong H, Zhang N, Leng Z, Li R & Gan S, *Colloids Surf*, A, 502 (2016) 139.
13 Sudheer G, Dadhich A S, Saha A & Saratchandra Babu M, *Rad Effects Defects Solids*, 170 (2016) 812.
14 Niu N, Yang P, Wang Y, Wang W, He F, Gai S & Wang D, *J Alloy Compd*, 509 (2011) 3096.
15 Dia W, Zhao X, Lu S, Wang X & Zhao H, *J Solid State Chem*, 180 (2007) 2478.
16 Day A & Purkait M K, *J Ind Eng Chem*, 24 (2015) 181.
17 Rai V N, Raja Sekhar B N, Kher S & Deb S K, *J Lumin*, 130 (2010) 582.
18 Vasil'ev A N, *IEEE Trans Nucl Sci*, 55 (2008) 1054.
19 Ruijie D T, Termini J & Gray H B, *J Med Chem*, 59 (2016) 6012.
20 Wu Y, Xu X, Li Q, Yang R, Ding H & Xiao Q, *J Rare Earths*, 33 (2015) 529.
21 Runowski M, Dabrowska K, Grzyb T, Miernikiewicz P & Lis S, *J Nanopart Res*, 15 (2013) 2068.
22 Di W, Li J, Shirahata N, Sakka Y, Willingere M & Pinna N, *Nanoscale*, 3 (2011) 1263.
23 Chavez K J, Garimella S V & Lipkowitz S, *Breast Dis,* 32 (2010) 35.
24 Guller A E, Generalova A N, Petersen E V, Nechaev A V, Trusova I A, Landyshev N N, Nadort A, Grebenik E A, Deyev S M, Shekhter A B & Zvyagin A V, *Nano Res*, 8 (2015) 1546.
25 Gayatri Devi V, Badana A, Kumari S, Nagaseshu P & Malla R R, *J Cancer Sci Ther*, 8 (2016) 104.
26 Han B, Zhang J, Liu B, Zhang J & Shi H, *Mater Lett*, 181 (2016) 305.
27 Boetter-Jensen L, McKeever S W S & Wintle A G, *Optically Stimulated Luminescence Dosimetry*, 1st Edn, (Elsevier Science BV, Amsterdam, The Netherlands), 2003.
28 Kun S, Peng X, Yongde M, Feng G, Jie L, Zhao L, James X, Jie C & Beihua K, *Int J Oncology*, 42 (2013) 597.